PCCP

PAPER

Cite this: *Phys. Chem. Chem. Phys.*, 2015, **17**, 23619

Inhibition effect of a non-permeating component on gas permeability of nanoporous graphene membranes†

Boyao Wen, Chengzhen Sun* and Bofeng Bai*

Received 3rd June 2015,
Accepted 7th August 2015

DOI: 10.1039/c5cp03195h

www.rsc.org/pccp

We identify the inhibition effect of a non-permeating gas component on gases permeating through the nanoporous graphene membranes and reveal its mechanisms from molecular dynamics insights. The membrane separation process involves the gas mixtures of CH_4/H_2 and CH_4/N_2 with different partial pressures of the non-permeating gas component (CH_4). The results show that the permeance of the H_2 and N_2 molecules decreases sharply in the presence of the CH_4 molecules. The permeance of the N_2 molecules can be reduced to as much as 64.5%. The adsorption of the CH_4 molecules on the graphene surface weakens the surface adsorption of the H_2 and N_2 molecules due to a competitive mechanism, accordingly reducing the permeability of the H_2 and N_2 molecules. For the N_2 molecules with stronger adsorption ability, the reduction of the permeance is greater. On the other hand, the CH_4 molecules near the nanopore have a blocking effect, which further inhibits the permeation of the H_2 and N_2 molecules. In addition, we predict the selectivity of the nanopore by using density functional theory calculations. This work can provide valuable guidance for the application of nanoporous graphene membranes in the separation of the gas mixtures consisting of permeating and non-permeating components with different adsorption abilities.

Introduction

Compared with the traditional gas separation technologies such as cryogenic distillation and pressure swing adsorption, membrane separation techniques have attracted more attention because of their advantages such as reliability, low energy consumption and need little investment on equipment.[1–4] Recent decades have witnessed the rapid development of membrane separation techniques, which are widely employed in the industrial separation processes. With the progress of nanoscience and technology, a series of nanostructured separation membranes have been developed such as zeolite,[5] carbon nanotubes[6] and graphene.[7] Graphene, a one-atom-thick sheet of graphite comprising sp^2-hybridized carbon atoms, has many fantastic properties, such as great mechanical strength, great thermal and electric conductivity, among others.[8–12] It is generally known that permeance and selectivity are two key parameters to evaluate a separation membrane, and permeance is generally inversely proportional to the thickness of the film. Owing to its one-atom thickness, graphene has shown a significant potential as a membrane in practical separation applications such as gas separation, water desalination,[13] and isotopes separation.[14] Previous studies have shown that pristine graphene is impermeable to gases,[10,15,16] even for gases as small as helium. However, graphene can be adopted as a selective gas separation film by introducing the nanopores with specific geometries and sizes, and is known as nanoporous graphene (NPG) membrane.[16]

Studies on gas separation through NPG membranes using different methods,[17–27] including theoretical analysis and experimental measurements, have suggested that the NPG membranes have great potential to become separation membranes with high permeance and selectivity. Jiang *et al.*[17] investigated the separation performance of a graphene sheet with designed sub-nanometer pores by first principles density functional theory calculations and found an extremely high selectivity for H_2/CH_4 with a high H_2 permeance. Their results indicated that the NPG membrane was far superior to the traditional gas separation membranes. Qin *et al.*[26] designed a NPG membrane with line defects consisting of a sequence of octagons and all-hydrogen passivated pores and showed that this membrane can efficiently separate the H_2/CH_4 gas mixture. Koening *et al.*[27] conducted the pressurized blister test and mechanical resonance to measure the transport rates of gases through the pores created by ultraviolet-induced oxidative etching and observed the selective transport of different gases. More excitingly, some graphene

State Key Laboratory of Multiphase Flow in Power Engineering, Xi'an Jiaotong University, Xi'an, Shaanxi, 710049, China.
E-mail: bfbai@mail.xjtu.edu.cn, sun-cz@mail.xjtu.edu.cn

† Electronic supplementary information (ESI) available. See DOI: 10.1039/c5cp03195h

synthesis and pore generation methods, such as chemical vapor deposition,[28] surface-assisted aryl–aryl coupling of cyclohexa-*m*-phenylene,[29] electron beam irradiation,[30] ultraviolet-induced oxidative etching,[31] and helium ion bombardment,[32] have been well developed to fabricate NPG membranes, helping make the gas separation using NPG membranes a reality.

In view of the difficulties in carrying out the experiments at nanometer scales, computer simulations have been widely used. Among them, the molecular dynamics (MD) simulation method,[33] which is based on the applicability of the laws of classical mechanics to microscopic systems, has been successfully employed to predict the macroscopic properties of many microscopic systems coupling with the rules of statistical mechanics. Several researchers have conducted the studies on the gas separation with NPG membranes using MD simulations.[34–43] The molecular adsorption on the graphene surface has a great impact on the gas permeation through the NPG membranes. Du *et al.*[42] designed a series of porous graphene membranes for separating the H_2/N_2 gas mixture and reported that the superior permeation of the N_2 molecules over that of the H_2 molecules when the pores were large enough owing to the strong adsorption of the N_2 molecules on the graphene surface. Drahushuk *et al.*[19] concluded the analytical expressions from several cases of the gas permeation through single layer graphene based on the molecular adsorption and used these mechanisms to predict the results reported by Du *et al.*[42] They also pointed out that the more strongly adsorbing N_2 permeates faster than the weakly adsorbing H_2. Sun *et al.*[43] further examined the surface adsorption phenomenon by MD simulations and proposed the mechanisms of molecular permeation through NPG membranes, where the total flux was divided into direct flux and surface flux. They found that the contribution of surface flux was even on the same order of magnitude of the total flux for the gases that strongly adsorbed onto graphene surfaces. Other studies have also been launched to reveal the effects of chemical functionalization on graphene sheets and nanopores,[38,44–46] the selectivity trend of different gas mixtures,[37,44] *etc*.

In summary, NPG membranes have shown extreme outstanding performance in gas separations. In the real industrial applications, the gas mixtures with different components are inevitably involved in the feed side of separation membranes. The existence of the non-permeating gas components may affect the permeation of the permeating gases and finally dominate the performance of the separation membranes. For the purpose of exploring a wide range of applications of the NPG membranes in gas separation industries, further study on the effects of the non-permeating gas components on the separation is urgently needed. To our knowledge, few studies on gas mixtures with different partial pressures have been conducted to analyze the effect of the non-permeating gas components on the gas permeability of NPG membranes from a microscopic viewpoint. In this paper, we employ the classical MD method to simulate the separation processes of the CH_4/H_2 and CH_4/N_2 gas mixtures with different partial pressures of the CH_4. We demonstrate that the presence of the CH_4 molecules tend to reduce the permeance of the H_2 and N_2 molecules due to the competitive adsorption mechanism and the blocking effect of the CH_4 molecules in the vicinity of the nanopores. This work indicates that the non-permeating component of the gas mixture affects the permeability of other gases in the mixture.

Model and methods

A cubic model was adopted to simulate the separation of a gas mixture using a NPG membrane, as shown in Fig. 1(a). The dimension of the square NPG membrane is 4×4 nm^2, making the membrane porosity equivalent to that of the actual prepared NPG membranes.[18,47] We positioned the graphene into a plane of $z = 0$ nm, dividing the simulation box into two chambers of equal volume. In order to prevent the vertical displacement of graphene caused by the collisions with gas molecules, one carbon atom in the membrane corner was fixed. The nanopore (see Fig. 1(b)) was created by selectively drilling some carbon atoms (we term it P-13, named after the removal

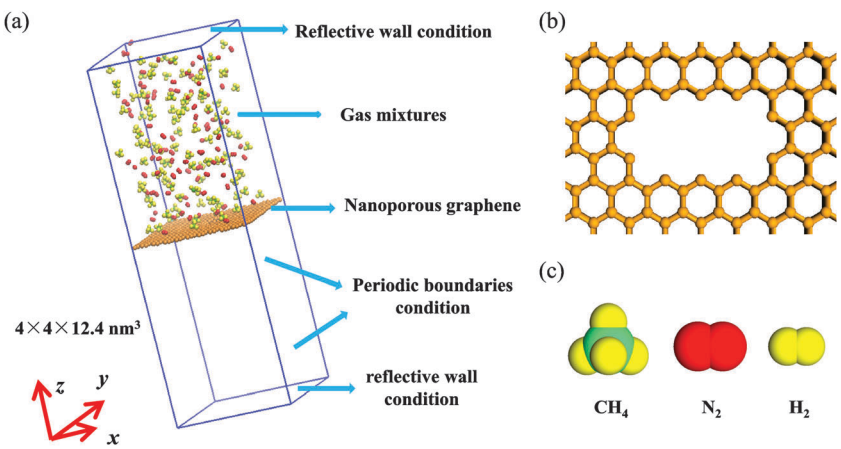

Fig. 1 Simulation model in our study. (a) Simulation box. (b) The structure of the nanopore employed in our simulations. This nanopore was termed P-13, named after the removal number of graphene ring units. (c) A scale model of the CH_4, N_2 and H_2 molecules.

number of graphene ring units). Although there will be some slight quantitative differences in the final results for different nanopores, this ideal nanopore is not expected to qualitatively affect the effect of the non-permeating gas component on the gas permeability of NPG membranes. Gas molecules were initially placed in a staggered way in one chamber 6.2 nm above the graphene membrane to obtain an initial pressure difference between the feed side and the permeating side. We chose the gas mixtures of the CH_4/H_2 and CH_4/N_2 (the molecular structures are shown in Fig. 1(c)) as the subjects of the study because the H_2 molecules and the N_2 molecules have quite different adsorption abilities. We expect that the non-permeating CH_4 molecules will have distinctive effects on the permeability of the molecules with different adsorption abilities. Four different partial pressures of the CH_4 molecules (listed in Table 1) were employed to explore the effects of the non-permeating gas component on the gas permeability. For convenience, we labelled them Cases 1–8 in turn. For the H_2 or N_2 molecules, the molecular number was kept constant to maintain a given initial partial pressure of 4.09 MPa; for the CH_4 molecules, the initial partial pressure varied from 0 to 6.14 MPa.

The MD simulations were performed using the LAMMPS package[48] in the NVT ensemble. A Nose–Hoover thermostat was used to maintain the system temperature equilibration at 300 K. Periodic boundary conditions were applied in the *x* and *y*-directions, while reflective boundary conditions were applied in the *z*-direction. We ran each simulation for 13.4 ns with a timestep of 0.134 fs. Before running the simulation, we performed the energy minimization to adjust the atomic coordinates in order to prevent the atomic overlap. The velocity-Verlet integration algorithm was used to obtain the molecular movement trajectories according to the Newton's second law of motion. The data of the atomic coordinates were printed every 2.5×10^4 timesteps to analyze the molecular permeation events and others. The C–C, C–H and H–H interactions were modeled using the AIREBO potential,[49] while the other interatomic interactions were modeled using the Lennard-Jones potential. The potential parameters between crossing atoms were obtained by using the Lorentz–Berthelot mixing rule. The potential models and the corresponding parameters are listed in Section S1.1 of the ESI.† The cutoff distance for AIREBO and Lennard-Jones potentials was 10 Å. The bond interactions of the CH_4 and H_2 molecules were included in the AIREBO potential, while those of N_2 molecules were modeled using the harmonic type potential (see ESI,† Section S1.2).

Table 1 Gas mixtures involved in this study (number of molecules). Cases 1–4 belong to CH_4/H_2 and Cases 5–8 belong to CH_4/N_2

	CH_4	H_2 or N_2
Case 1	0	100
Case 2	50	100
Case 3	100	100
Case 4	150	100
Case 5	0	100
Case 6	50	100
Case 7	100	100
Case 8	150	100

Results and discussion

Molecular permeation

A molecule moving from the original side to the other side is termed a permeation event. The number of the permeated molecules *versus* time can be acquired through the analysis of molecular trajectories (see Fig. S1 and S2 in Section S2 of the ESI†). It is obvious that the H_2 and N_2 molecules can permeate smoothly through the nanopore while the CH_4 molecules can hardly pass through it. This phenomenon is consistent with the size sieving separation mechanism. Owing to its elliptic shape, the nanopore P-13 in our study can more efficiently hinder the CH_4 molecules from permeating in the minor axis direction. This unique characteristic of P-13 makes our study feasible on the effect of the non-permeating CH_4 molecules on the separation processes of the CH_4/H_2 and CH_4/N_2 gas mixtures.

Based on the definitions of flux and permeance, a theoretical model of the time-dependent number of the permeated molecules is deduced. The relationship between a flux J (mol s^{-1}) and a permeance S (mol s^{-1} m^{-2} Pa^{-1}) can be expressed as

$$J = \frac{1}{N_A}\frac{dN}{d\tau} = A_g \cdot \Delta P \cdot S \quad (1)$$

where A_g is the area of the graphene used in our simulations ($A_g = 1.6 \times 10^{-17}$ m^2), ΔP is the pressure difference between the two sides of the NPG, S is the gas permeance, N is the number of the permeated gas molecules, τ is the time and N_A is the Avogadro constant. The pressure difference ΔP depends on the permeated molecular number N. For example, for H_2 and N_2 with an initial partial pressure of 4.09 MPa,

$$\Delta P = \frac{100 - N_a - 2N}{100} \times 4.09 \times 10^6 \text{ Pa} \quad (2)$$

where N_a is the average number of the gas molecules adsorbed on the adsorption layer (-0.6 nm $\leq z \leq$ 0.6 nm).[43] By integrating eqn (1), we obtain

$$N = (50 - N_a/2) \times (1 - e^{-7.88 \times 10^{11} S\tau}) \quad (3)$$

where $B = 7.88 \times 10^{11} S$ is the exponent of time decay. For CH_4 in different cases, the relationship between B and S is different owing to the different initial partial pressures.

Then, we apply eqn (3) to fit the curves given by the number of the permeated molecules *versus* time and obtain the permeance of different molecules. For instance, Fig. S3 of the ESI† shows the fitting curve of N for the molecule N_2 *versus* time in Case 5. The fitted parameter $B = 7.88 \times 10^{11} S = 1.64 \times 10^8$, and then we can obtain the permeance of N_2 in Case 5, *i.e.*, $S_{\text{Case 5}} = 2.08 \times 10^{-4}$ mol s^{-1} m^{-2} Pa^{-1}. Similarly, we can obtain the gas permeance in other cases. It is noted that the fitting was only carried out for the process before the permeation of the molecules reaching the equilibrium. The permeance of all the molecules and their fitted standard errors are listed in Table S2 of the ESI.† We find that the gas permeance is four orders of magnitude higher than that of the traditional polymer membranes ($\sim 10^{-8}$ mol s^{-1} m^{-2} Pa^{-1}).[50]

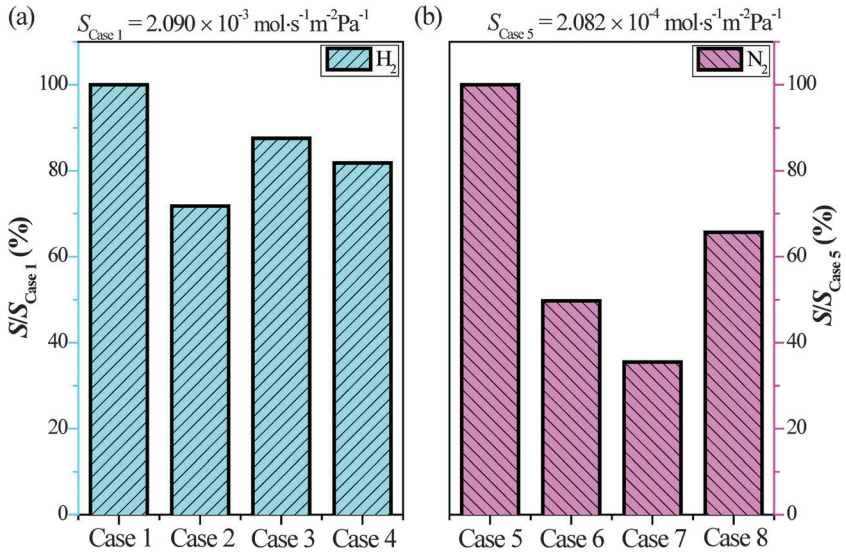

Fig. 2 Permeances of the H_2 and N_2 molecules. (a) The normalized parameter $S/S_{Case\,1}$ of the H_2 molecules in Cases 1–4. (b) The normalized parameter $S/S_{Case\,5}$ of the N_2 molecules in Cases 5–8.

In order to precisely quantify the influence of the non-permeating gas component on the molecular permeation, we adopt the dimensionless parameters $S/S_{Case\,1}$ and $S/S_{Case\,5}$ (Case 1 and Case 5 are the cases without CH_4) for further analysis, as shown in Fig. 2. As seen from the figure, the permeance of the H_2 and N_2 molecules reduces obviously owing to the presence of the non-permeating CH_4 molecules. Their reduction is different at different partial pressures of CH_4. The permeance of the N_2 molecules reduces to as much as 64.5%, surpassing the H_2 molecules by far, which reduces to 28.2%. The reasons for their distinctive reduction will be discussed below. According to the permeance, the selectivity of this nanopore for two kinds of gas molecules can be obtained using $F_{A/B} = S_A/S_B$. In our simulations, we observe that typically only one or two CH_4 molecules can pass through the nanopore, and no crossing events occur in Case 2. In the case of zero molecular penetration, the molecular permeated number is assumed to be 1 in the calculation of the selectivity. In our simulations, the simulated selectivity of the nanopore for H_2/CH_4 is of the order of 10^2, while that for N_2/CH_4 is of the order of 10, as shown in Fig. S4 of the ESI.†

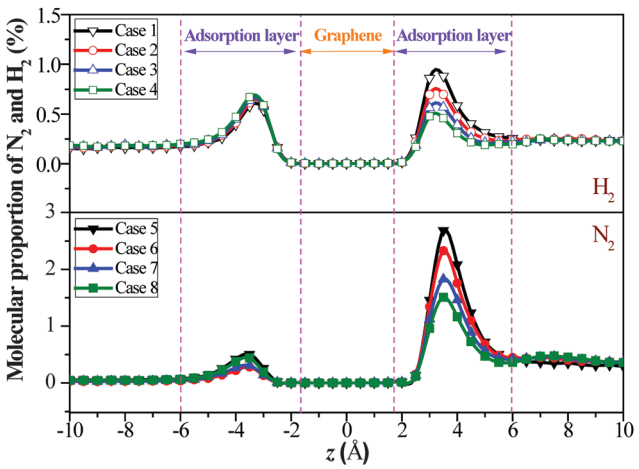

Fig. 3 Density distribution along the z-direction for the H_2 and N_2 molecules. A molecular surface adsorption phenomenon was found and an adsorption layer was defined, which consisted of 1.7 Å $< z \leq$ 6 Å and -6 Å $\leq z <$ -1.7 Å regions. The open symbols: H_2 molecules; the solid symbols: N_2 molecules.

Surface adsorption

According to the simulation results, we can obtain the time-averaged density distributions of the gas molecules along the z-direction, as shown in Fig. 3. The greater density of the gas molecules near the graphene means that the molecules are adsorbed on the graphene surface and form an adsorption zone. This zone of about one molecule thick is termed adsorption layer which is caused by the strong van der Waals force between the molecules and the carbon atoms of the graphene. Because the gas molecules are initially arranged in one side of the graphene, the density of the molecules in the initial side is greater than that in the permeating side. We also find that the proportion of the N_2 molecules in the adsorption layer is about twice as much as that of the H_2 molecules, owing to the stronger interactions between the N_2 molecules and the carbon atoms of the NPG.

A noteworthy phenomenon is that with the increase of the number of the CH_4 molecules, the proportion of the H_2 or N_2 molecules in the adsorption layers decreases. In order to reveal the reasons for this phenomenon, we performed a statistical analysis of the average number of the gas molecules in the adsorption layers (N_a) (1.7 Å $< z \leq$ 6 Å and -6 Å $\leq z <$ -1.7 Å regions). The N_a of gas molecules is related to the pore structure, chemical modifications, and the porosity of graphene membranes as well as the components of the gas mixtures. As shown in Fig. 4, the N_a of the CH_4 molecules increases linearly with the increase of its partial pressure while the N_a of the H_2 and

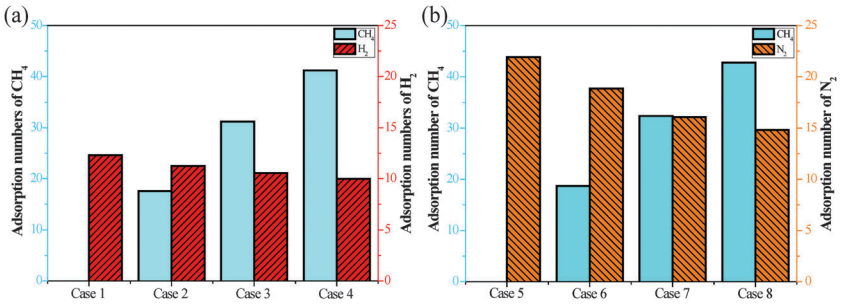

Fig. 4 Average adsorbed number (N_a) of gas molecules in the adsorption layer during the simulation time. (a) Average adsorbed number (N_a) of the H_2 and CH_4 molecules in the adsorption layer in Cases 1–4. (b) Average adsorbed number (N_a) of the N_2 and CH_4 molecules in the adsorption layer in Cases 5–8.

N_2 molecules decreases gradually. This opposite trend results from the competitive adsorption of the CH_4 and the H_2 or N_2 molecules on the surface of the graphene. The adsorption ability of the CH_4 molecules on the graphene is greater than that of the N_2 and H_2 molecules. The CH_4 molecules occupy the space of the adsorption layers and drive the H_2 and N_2 molecules out of the adsorption layers, thus reducing the N_a of the H_2 and N_2 molecules. The descending ratio of the N_2 molecules is greater than that of the H_2 molecules, indicating the greater impact of the CH_4 molecules on the adsorption of the N_2 molecules. The greater reduction in the N_a of N_2 is related to its stronger adsorption ability compared to the H_2 molecules. The adsorption ability can also be demonstrated from the maximum adsorption time (MAT), *i.e.* the time period for which a molecule continuously stays in the adsorption layer, as shown in Fig. 5. The MAT of the H_2 molecules decreases sharply because of the intervention of the CH_4 molecules, while the MAT of the N_2 molecules remains nearly constant for their stronger adsorption ability. Typically, the residence time of the N_2 molecules in the adsorption layer is longer than that of H_2.

The adsorption ability of the gas mixture is positively correlated with partial pressure of gases, and the competing adsorption phenomenon occurs on the surface of the graphene, which is caused by the different adsorption abilities of the components in the gas mixture. As stated previously, the CH_4 molecules occupy the adsorption layers, thus reducing the N_a of the H_2 and N_2 molecules. The reduction of the N_a for N_2 molecules with stronger adsorption ability is greater. According to the mechanism proposed by Sun *et al.*,[43] for gases that strongly adsorb onto the graphene surface, the surface flux in which the molecules permeate after being adsorbed on the surface of the graphene has a significant contribution to the total flux and is directly related to the molecular adsorption intensity. For the N_2 molecules, because of the significant contribution of the surface flux to the total flux, the greater reduction of N_a induces a lower surface flux and finally results in a greater reduction of the total flux and permeance. For the H_2 molecules, the reduction of N_a is smaller and the surface flux has a little contribution to the total flux, and thus the reduction of the total flux and permeance is smaller.

Molecular blocking

Fig. 6 displays the density distributions of the H_2, N_2 and CH_4 molecules in the adsorption layer. We assume that the molecules distribute uniformly in the z-direction and thus the molecular density is only a function of the distance R between the molecule and the nanopore center parallel to the graphene plane. Given that the side of a NPG membrane is 4 nm long, the molecules in the adsorption layer get rare when R is higher than 18 Å, so we do not show this region in the figure. Based on the characteristics of the curves in Fig. 6, the adsorption layer can be divided into two regions: $0 < R \leq 10$ Å and 10 Å $< R \leq 18$ Å, named as region I and region II, respectively. The fractions of the H_2 and N_2 molecules near the nanopore (region I) are usually lower than the fractions far away from the nanopore (region II), due to the permeation event of molecules. This phenomenon is also related to the lack of the graphene–carbon-atom in region I, which similarly results in a lower fraction of the CH_4 molecules near the nanopore (region I). In region I,

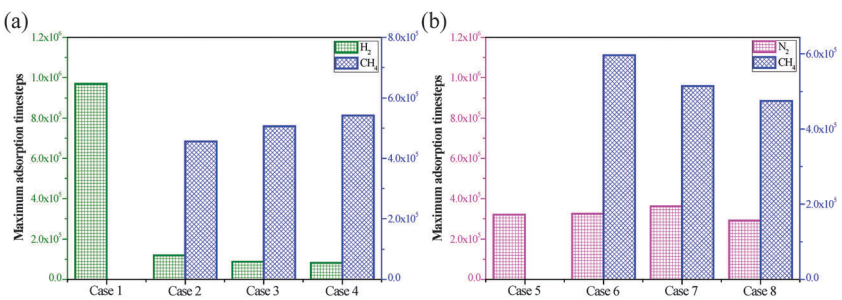

Fig. 5 Maximum adsorption timesteps (MAT) of the gas molecules in the adsorption layer. (a) MAT of the H_2 and CH_4 molecules in the adsorption layers in Cases 1–4. (b) MAT of the N_2 and CH_4 molecules in the adsorption layers in Cases 5–8.

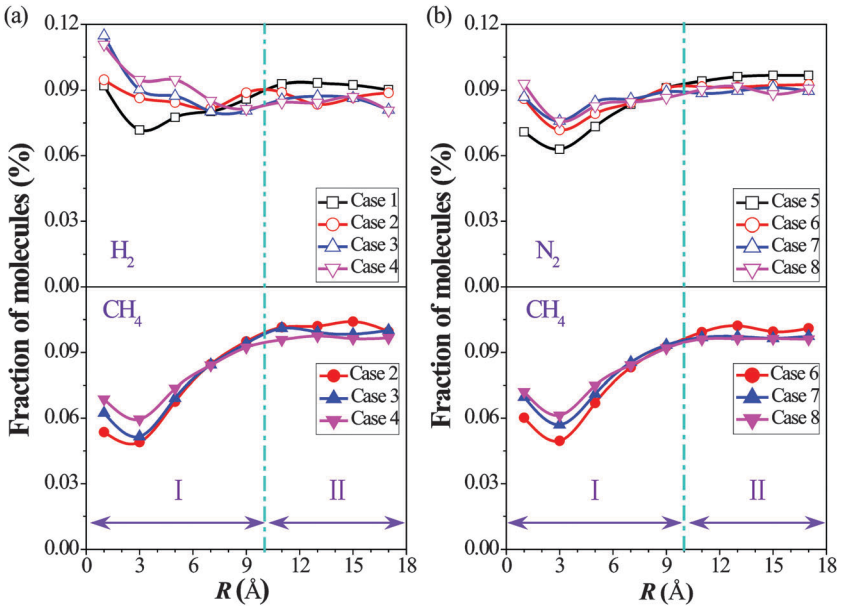

Fig. 6 Density distributions of the gas molecules in the adsorption layers *versus* R. (a) Density distributions of the H_2 and CH_4 molecules in the adsorption layers *vs.* R. Open symbols: H_2; solid symbols: CH_4. (b) Density distributions of the N_2 and CH_4 molecules in the adsorption layers *vs.* R. Open symbols: N_2; solid symbols: CH_4. The adsorption layer is divided into two regions (I and II). Region I is 0 Å $< R \leq$ 10 Å and region II is 10 Å $< R \leq$ 18 Å.

with the increase of partial pressure of the CH_4 molecules, the density of the CH_4 molecules near the nanopore increases. Accordingly, the density of the H_2 and N_2 molecules near the nanopore center also increases, because the blocking effect of the CH_4 molecules makes it hard for other components to permeate and their permeation is delayed. In region II, the density of the H_2 and N_2 molecules in the adsorption layer decreases in the presence of the CH_4 molecules. This is due to the competing adsorption of the gas mixture, as illustrated in the Surface adsorption section. In other words, the permeation of the H_2 and N_2 molecules through the nanopore is inhibited significantly by the presence of the CH_4 molecules which block the nanopore and hinder the crossing of the H_2 and N_2 molecules. Consequently, a reduction of the permeance of the H_2 and N_2 molecules appears.

We also introduce a parameter α to describe the movement of molecules in the course of molecular permeation. The parameter α is defined as the angle between the z-axis rotating in the clockwise direction and the connected line of atomic centers in the molecule, as shown in the inset map in Fig. 7(a). This figure shows the variation of the angle α when a H_2 molecule in Case 1 permeates through the nanopore. Because the thickness of the graphene is 0.34 nm, the plane of $z = 0.17$ nm is the mark to indicate the entrance of the molecule in the nanopore. As the z-position of the molecule decreases to 0.17 nm, the corresponding angle α is denoted as θ. We find that the angle α decreases gradually until the molecule reaches the nanopore. This means that the molecule tends to position itself to be perpendicular to the graphene plane before entering the nanopore. After the molecule successfully enters into the nanopore, the angle

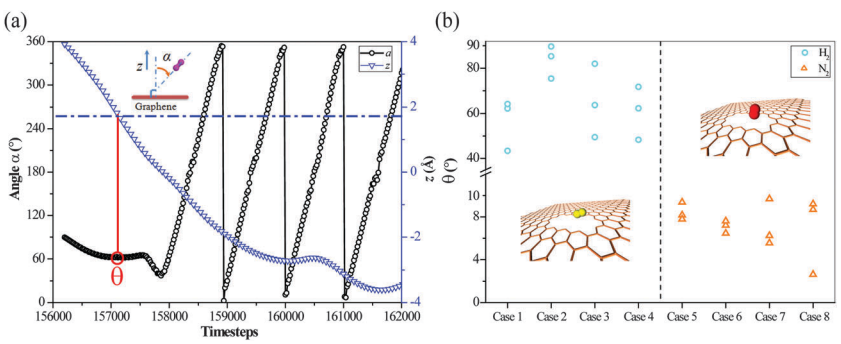

Fig. 7 Variations of the angle α of the molecule in the course of permeation and the scattergram of θ for all cases. (a) The time-dependent variation of angle α for the H_2 molecule permeating through the nanopore. Black circular symbols: α; blue inverted triangle symbols: z; the inset map represents the definition of angle α; red circle represents the θ. (b) The scattergram of θ for all cases. We obtained the value of θ from the first three crossings for the H_2 and N_2 molecules in Cases 1–8. The inset in the lower-left corner of the figure is the atomic view of a H_2 molecule permeating the nanopore; the inset in the top-right corner of the figure is the atomic view of a N_2 molecule permeating the nanopore.

α shows periodical variations because of the self-rotation of the molecule, which may be caused by the collisions between the molecule and the graphene. In other cases, the variations of the angle α have similar trends. Therefore, θ is an important parameter to define the permeation of the molecule through the nanopore. From the first three crossings for H_2 and N_2 in Cases 1–8, we obtain the value of θ, as shown in Fig. 7(b). It is obvious that the θ of the N_2 molecules is smaller than that of the H_2 molecules, meaning that the N_2 molecules tend to permeate through the nanopore with an angle nearly perpendicular to the graphene plane due to their bigger size. Meanwhile, the variation range of θ for the N_2 molecules is also smaller than that of the H_2 molecules. It means that the N_2 molecules only can permeate through the nanopore in a special orientation while the H_2 molecules can permeate in a wide range of orientations.

Interaction energy

The selectivity of the nanopore concluded from the simulation results is shown in Fig. S4 of the ESI.† We find that the effect of partial pressure on the selectivity of the nanopore is negligible, which indicates that the selectivity is mainly determined by the features of the nanopore and the gas mixture. Therefore, we further calculate the interaction energy between the gas molecule and the NPG by using the Dmol^3 module in the Material Studio software,[51] as shown in Fig. 8. For the H_2 and N_2 molecules, we take the molecular configuration, that the connected line of atomic centers in the molecule is perpendicular to the graphene plane, to conduct the calculations; for CH_4 molecule, the angle of the four H atoms pointing toward the four corners of the nanopore is adopted.[17,38] According to the interaction energy, we can obtain the diffusion barriers and accordingly estimate the selectivity of this nanopore by using the Arrhenius equation. The estimation method of the selectivity for separating the H_2/CH_4 and N_2/CH_4 gas mixtures can be found in Section S3.2 of the ESI.† The different diffusion barriers of the H_2, N_2 and CH_4 molecules yield an extremely high selectivity of 10^{12} for the H_2/CH_4 gas mixture, while a selectivity of only 26.73 for the N_2/CH_4 gas mixture. The estimated selectivity for the N_2/CH_4 gas mixture is nearly equivalent to the simulated value, but the estimated selectivity for the H_2/CH_4 gas mixture far surpasses the simulated selectivity. These estimated selectivities are comparable with those in the previous study.[17,20] We consider the nanopore as unrelaxed in density functional calculations but flexible in molecular dynamics simulations. The geometry distortion of the flexible nanopore caused by the permeation of gas molecules may decrease the selectivity significantly, as illustrated by Hauser and Schwerdtfeger.[20] Thus, the higher estimated selectivity for the H_2/CH_4 gas mixture can be partly attributed to the unrelaxed pores in our density functional calculations. In addition, we compare the diffusion barriers for the transition of the CH_4, N_2 and H_2 molecules in our results with those of a previous study[20] (see Section S3.3 of the ESI† for more details). The above study demonstrates that this nanopore possesses high selectivity for the H_2/CH_4 and N_2/CH_4 gas mixtures, meaning that the NPG membranes can be used as efficient membranes to separate gas mixtures with specific nanopores.

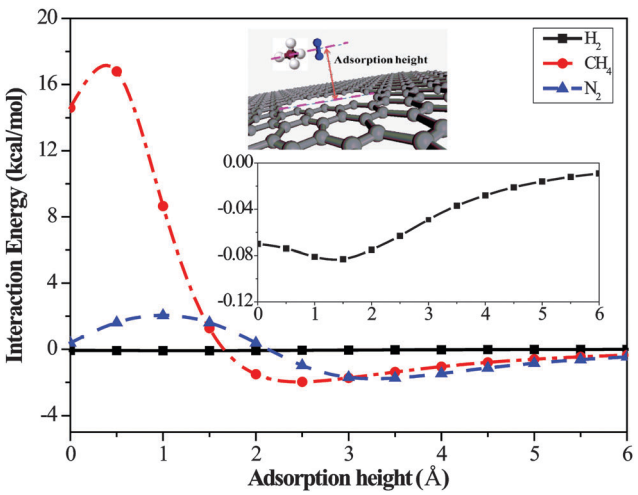

Fig. 8 Interaction energy of the H_2, N_2 and CH_4 molecules *versus* adsorption height. The top inset map shows the definition of the adsorption height. The bottom inset map is the enlarge view of the H_2 curve.

Conclusions

The gas mixtures of CH_4/H_2 and CH_4/N_2 with different partial pressures of the non-permeating gas component (CH_4) are adopted to explore the effect of the non-permeating gas component on gas permeability of NPG membranes by molecular dynamics simulations. The results show that the permeation of the H_2 and N_2 molecules is inhibited significantly by the CH_4 molecules, which can be attributed to two aspects: the relatively decreasing contribution of the surface adsorption and the blocking effect of the CH_4 molecules in the vicinity of the nanopore. Namely, the presence of the non-permeating CH_4 molecules causes the weakening of the surface adsorption of H_2 and N_2, thus limiting their permeation ability. For the N_2 molecules with stronger adsorption ability, the weakening extent of the surface adsorption is greater. Meanwhile, the CH_4 molecules near the nanopore can block the permeation of H_2 and N_2 molecules. Moreover, by analyzing the variations of the angle between the connected line of the atomic centers and the perpendicular orientation of the graphene in the course of the molecular crossing, we find that the N_2 molecules can only permeate through the nanoporous graphene membranes in a special orientation because of their bigger size.

In summary, our study identifies the inhibition effect of a non-permeating gas component on the gas permeability of nanoporous graphene membranes. The mechanisms concluded from a theoretical point of view may be helpful to explain the phenomena observed in the future experimental studies. Meanwhile, we hope that this work can provide guidance for the application of the NPG membranes in the industrial gas separation processes.

Acknowledgements

This work was supported by the National Natural Science Foundation of China for Distinguished Young Scientists (No. 51425603) and key program (No. 51236007).

References

1 H. Strathmann, *J. Membr. Sci.*, 1981, **9**, 121–189.
2 R. W. Baker, E. Cussler, W. Eykamp, W. Koros, R. Riley and H. Strathmann, *Membrane separation systems: recent developments and future directions*, Noyes Data Corporation Park Ridge, NJ, 1991.
3 P. Bernardo, E. Drioli and G. Golemme, *Ind. Eng. Chem. Res.*, 2009, **48**, 4638–4663.
4 R. W. Baker, *Ind. Eng. Chem. Res.*, 2002, **41**, 1393–1411.
5 K. Na, C. Jo, J. Kim, K. Cho, J. Jung, Y. Seo, R. J. Messinger, B. F. Chmelka and R. Ryoo, *Science*, 2011, **333**, 328–332.
6 B. J. Hinds, N. Chopra, T. Rantell, R. Andrews, V. Gavalas and L. G. Bachas, *Science*, 2004, **303**, 62–65.
7 A. K. Geim and K. S. Novoselov, *Nat. Mater.*, 2007, **6**, 183–191.
8 A. K. Geim, *Science*, 2009, **324**, 1530–1534.
9 Y. Zhu, S. Murali, W. Cai, X. Li, J. W. Suk, J. R. Potts and R. S. Ruoff, *Adv. Mater.*, 2010, **22**, 3906–3924.
10 L. Tsetseris and S. Pantelides, *Carbon*, 2014, **67**, 58–63.
11 A. Kumar, A. L. M. Reddy, A. Mukherjee, M. Dubey, X. Zhan, N. Singh, L. Ci, W. E. Billups, J. Nagurny and G. Mital, *ACS Nano*, 2011, **5**, 4345–4349.
12 K. I. Bolotin, K. Sikes, Z. Jiang, M. Klima, G. Fudenberg, J. Hone, P. Kim and H. Stormer, *Solid State Commun.*, 2008, **146**, 351–355.
13 D. Cohen-Tanugi and J. C. Grossman, *Nano Lett.*, 2012, **12**, 3602–3608.
14 A. W. Hauser, J. Schrier and P. Schwerdtfeger, *J. Phys. Chem. C*, 2012, **116**, 10819–10827.
15 V. Berry, *Carbon*, 2013, **62**, 1–10.
16 J. S. Bunch, S. S. Verbridge, J. S. Alden, A. M. van der Zande, J. M. Parpia, H. G. Craighead and P. L. McEuen, *Nano Lett.*, 2008, **8**, 2458–2462.
17 D.-E. Jiang, V. R. Cooper and S. Dai, *Nano Lett.*, 2009, **9**, 4019–4024.
18 M. S. Boutilier, C. Sun, S. C. O'Hern, H. Au, N. G. Hadjiconstantinou and R. Karnik, *ACS Nano*, 2014, **8**, 841–849.
19 L. W. Drahushuk and M. S. Strano, *Langmuir*, 2012, **28**, 16671–16678.
20 A. W. Hauser and P. Schwerdtfeger, *Phys. Chem. Chem. Phys.*, 2012, **14**, 13292–13298.
21 H. W. Kim, H. W. Yoon, S.-M. Yoon, B. M. Yoo, B. K. Ahn, Y. H. Cho, H. J. Shin, H. Yang, U. Paik, S. Kwon, J.-Y. Choi and H. B. Park, *Science*, 2013, **342**, 91–95.
22 K. Nieszporek and M. Drach, *Phys. Chem. Chem. Phys.*, 2015, **17**, 1018–1024.
23 K. Celebi, J. Buchheim, R. M. Wyss, A. Droudian, P. Gasser, I. Shorubalko, J.-I. Kye, C. Lee and H. G. Park, *Science*, 2014, **344**, 289–292.
24 C. Huang, H. Wu, K. Deng, W. Tang and E. Kan, *Phys. Chem. Chem. Phys.*, 2014, **16**, 25755–25759.
25 B. J. Bucior, D.-L. Chen, J. Liu and J. K. Johnson, *J. Phys. Chem. C*, 2012, **116**, 25904–25910.
26 X. Qin, Q. Meng, Y. Feng and Y. Gao, *Surf. Sci.*, 2013, **607**, 153–158.
27 S. P. Koenig, L. Wang, J. Pellegrino and J. S. Bunch, *Nat. Nanotechnol.*, 2012, **7**, 728–732.
28 M.-Y. Lin, C.-F. Su, S.-C. Lee and S.-Y. Lin, *J. Appl. Phys.*, 2014, **115**, 223510.
29 P. Kuhn, A. Forget, D. Su, A. Thomas and M. Antonietti, *J. Am. Chem. Soc.*, 2008, **130**, 13333–13337.
30 M. D. Fischbein and M. Drndić, *Appl. Phys. Lett.*, 2008, **93**, 113107.
31 S. Huh, J. Park, Y. S. Kim, K. S. Kim, B. H. Hong and J.-M. Nam, *ACS Nano*, 2011, **5**, 9799–9806.
32 D. C. Bell, M. C. Lemme, L. A. Stern, J. R. Williams and C. M. Marcus, *Nanotechnology*, 2009, **20**, 455301.
33 D. C. Rapaport, *The art of molecular dynamics simulation*, Cambridge University Press, 2004.
34 H. Liu, S. Dai and D.-e. Jiang, *Nanoscale*, 2013, **5**, 9984–9987.
35 N. Inui, K. Mochiji, K. Moritani and N. Nakashima, *Appl. Phys. A: Mater. Sci. Process.*, 2010, **98**, 787–794.
36 Q. Xue, M. Shan, Y. Tao, Z. Liu, C. Ling and Y. Du, *Chin. Sci. Bull.*, 2014, **59**, 3919–3925.
37 H. Liu, Z. Chen, S. Dai and D.-E. Jiang, *J. Solid State Chem.*, 2015, **224**, 2–6.
38 T. Wu, Q. Xue, C. Ling, M. Shan, Z. Liu, Y. Tao and X. Li, *J. Phys. Chem. C*, 2014, **118**, 7369–7376.
39 G. Lei, C. Liu, H. Xie and F. Song, *Chem. Phys. Lett.*, 2014, **599**, 127–132.
40 B. Y. Wen, C. Z. Sun and B. F. Bai, *Acta Phys. – Chim. Sin.*, 2015, **31**, 261–267.
41 C. Sun, F. Zhang, H. Liu and B. Bai, *CIESC J.*, 2014, **65**, 3026–3031.
42 H. Du, J. Li, J. Zhang, G. Su, X. Li and Y. Zhao, *J. Phys. Chem. C*, 2011, **115**, 23261–23266.
43 C. Sun, M. S. Boutilier, H. Au, P. Poesio, B. Bai, R. Karnik and N. G. Hadjiconstantinou, *Langmuir*, 2014, **30**, 675–682.
44 M. Shan, Q. Xue, N. Jing, C. Ling, T. Zhang, Z. Yan and J. Zheng, *Nanoscale*, 2012, **4**, 5477–5482.
45 J. Schrier, *ACS Appl. Mater. Interfaces*, 2011, **3**, 4451–4458.
46 X. Huang, K. Qian, J. Yang, J. Zhang, L. Li, C. Yu and D. Zhao, *Adv. Mater.*, 2012, **24**, 4419–4423.
47 S. C. O'Hern, C. A. Stewart, M. S. Boutilier, J.-C. Idrobo, S. Bhaviripudi, S. K. Das, J. Kong, T. Laoui, M. Atieh and R. Karnik, *ACS Nano*, 2012, **6**, 10130–10138.
48 S. Plimpton, P. Crozier and A. Thompson, *LAMMPS-large-scale atomic/molecular massively parallel simulator*, Sandia National Laboratories, 2007.
49 S. J. Stuart, A. B. Tutein and J. A. Harrison, *J. Chem. Phys.*, 2000, **112**, 6472–6486.
50 H. B. Park, C. H. Jung, Y. M. Lee, A. J. Hill, S. J. Pas, S. T. Mudie, E. Van Wagner, B. D. Freeman and D. J. Cookson, *Science*, 2007, **318**, 254–258.
51 F. Module, *Material Studio 6.0*, Accelrys Inc., San Diego, CA, 2011.